Proc. of SPIE Vol. 1167, Precision Engineering and Optomechanics, ed. D Vukobratovich (Nov 1989) Copyright SPIE

Structural dynamic analysis of laser spot motion in xerographic printers

Bill Nowak

Xerox Corporation, 800 Phillips Road, Webster, New York 14580

ABSTRACT

This paper describes the application of finite element analysis to calculate the dynamic response of a xerographic laser printer write head known as a "raster output scanner" (ROS). Steady and transient dynamic loading conditions are applied to a structural model of the ROS component support casting which has mathematical relationships accounting for the opto-mechanical interaction of 14 laser spot conditioning lenses and mirrors with the mounting structure. The output of the these relationships describe the dynamic response of the laser spot at the photoconductor surface. The response amplitude is then compared to a motion specification to determine if perceptible defects in xerographic prints will occur.

2. INTRODUCTION

As the customer demand for quality high speed computer output devices increases, so do the engineering requirements placed on the design and manufacturing of these systems. Shorter design cycle time, cost effective designs and high quality output prints make it necessary to perform higher order analyses on these products to be competitive in today's marketplace. The analysis of structural dynamics in laser printers is one of several areas where the motion effects on laser beam spot placement need be well understood so these products will produce high quality xerographic prints.

This paper briefly describes how a xerographic printer works, the structural motion quality problems which effect output print quality and the print quality failure criteria called "banding." The structural dynamic analysis approach, which includes the finite element modeling strategy and empirical model validation, is developed in detail. The results of the analyses are presented and compared to print quality failure data, and recommendations on future work are cited.

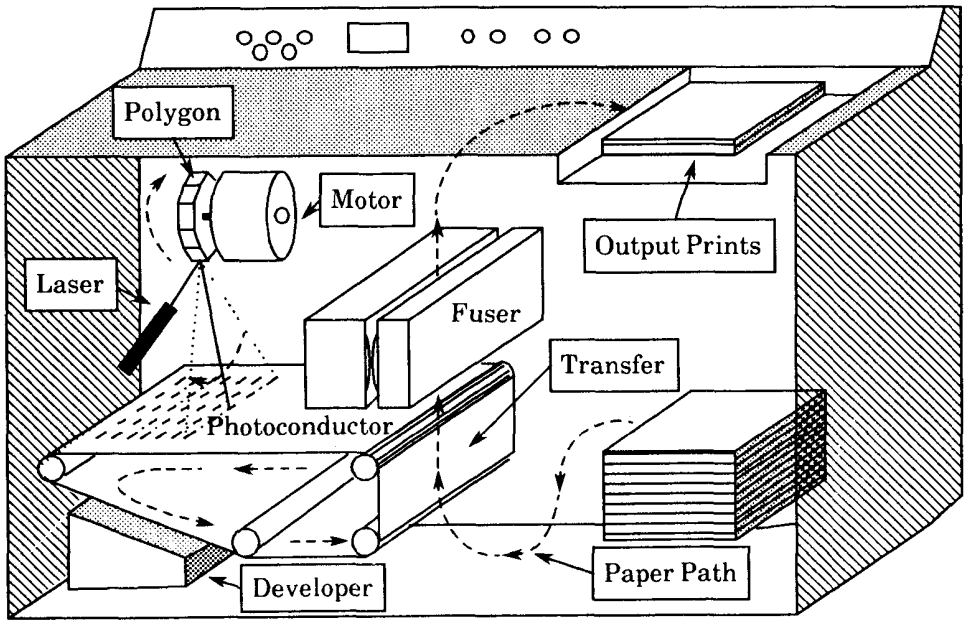

Figure 1 Schematic of a typical xerographic laser printer.

3. LASER PRINTER FUNDAMENTALS

Shown in Figure 1 is a schematic of a typical xerographic laser printer. A laser beam is scanned across a charged photoconductor by a spinning polygon mirror, and a digital electrostatic image is formed. The moving photoconductor belt carries the image through the developer, where "dry ink" adheres to the charged areas, and then to the transfer area where the dry ink is electrostatically transferred to plain paper. The paper with the developed image then continues through the fuser, where the dry ink is fused to the paper typically with a combination of heat and uniformly applied pressure. The finished print then continues to an output tray or through a finishing device such as a binder or sorter.

There is significantly more technological detail in the laser/polygon region of Figure 1. The write head, referred to as a raster output scanner (ROS), is composed of many output beam conditioning lenses and turning mirrors used to fold the required optical path length into a structure of manageable size as shown in Figure 2. A beam is emitted from a helium-neon laser, through a series of pre-polygon conditioning lenses and

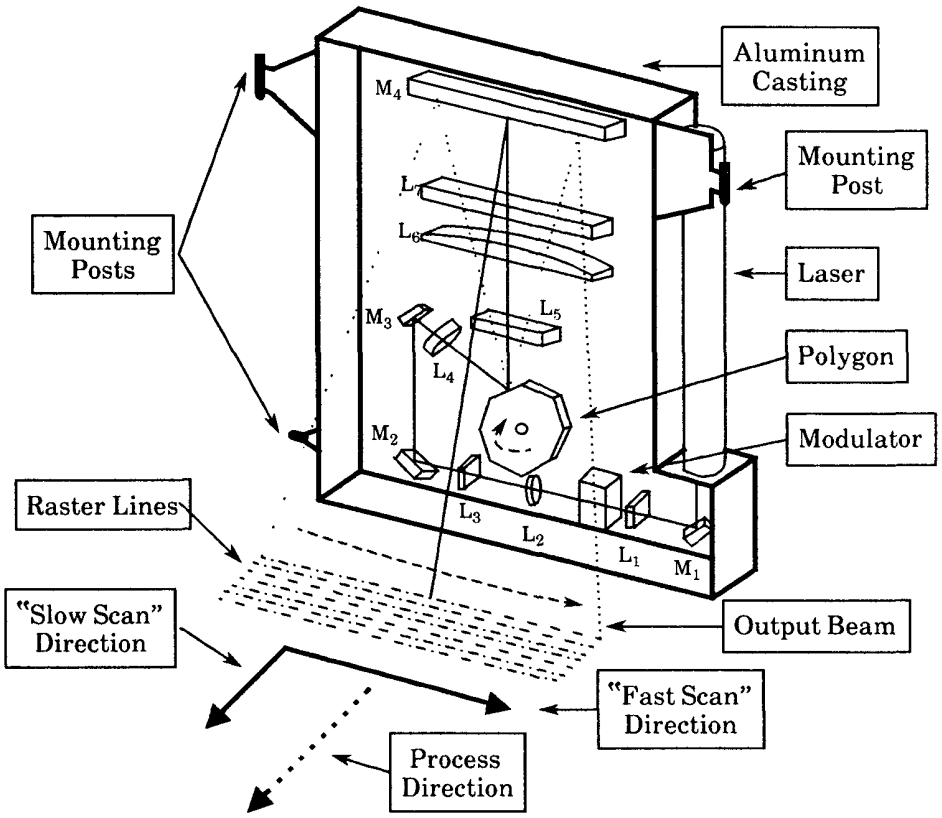

Figure 2. Schematic of a raster output scanner (ROS).

turning mirrors, onto the rotating polygon mirror. The high speed rotation of the polygon, which is usually in the 3 to 15 krpm range, then scans the beam through a series of post-polygon conditioning lenses and onto a final turning mirror, and images the laser spot across the full process width at the image plane as the photoconductor surface passes by. An electronic subsystem, which processes the digital information, directs the modulator to deflect the laser beam "on to" or "off of" a light stop which turns the laser spot on or off at the photoconductor surface The laser beam discharges areas on the photoconductor where dry ink is not intended to adhere, leaving areas charged where dry ink is intended to adhere.

There are many sources of excitation within the confines of a xerographic printer or applied to the printer by its environment. Because the ROS is attempting to write images on the photoconductor while these excitations are present, it is reasonable to assume that these disturbances will transmit through the frame and to the ROS casting, and cause the optical elements to respond at various amplitudes. The resulting opto-mechanical coupling of the optics and the casting causes the ROS spot to move relative to the photoconductor surface. This relative motion is defined as "image motion." The frequency and amplitude of this motion will determine if print quality degradation due to structural vibration is expected.

4. PRINT FAILURE CRITERIA

The failure criteria used to evaluate the severity of image motion and its effects on print quality is called "banding." This digital image phenomena is shown in Figure 3 where the spacing of vertical lines (perpendicular to the process direction) are sinusoidally varied by a velocity error, $\delta V_{0\text{-}Peak}$, causing light and dark areas to occur in output prints. Banding is related to vibratory errors in the process or slow scan direction with the bands always being aligned perpendicular to the slow scan direction as shown in figure 3. This phenomena is even more perceptible when viewing prints made up of digitized halftone areas.

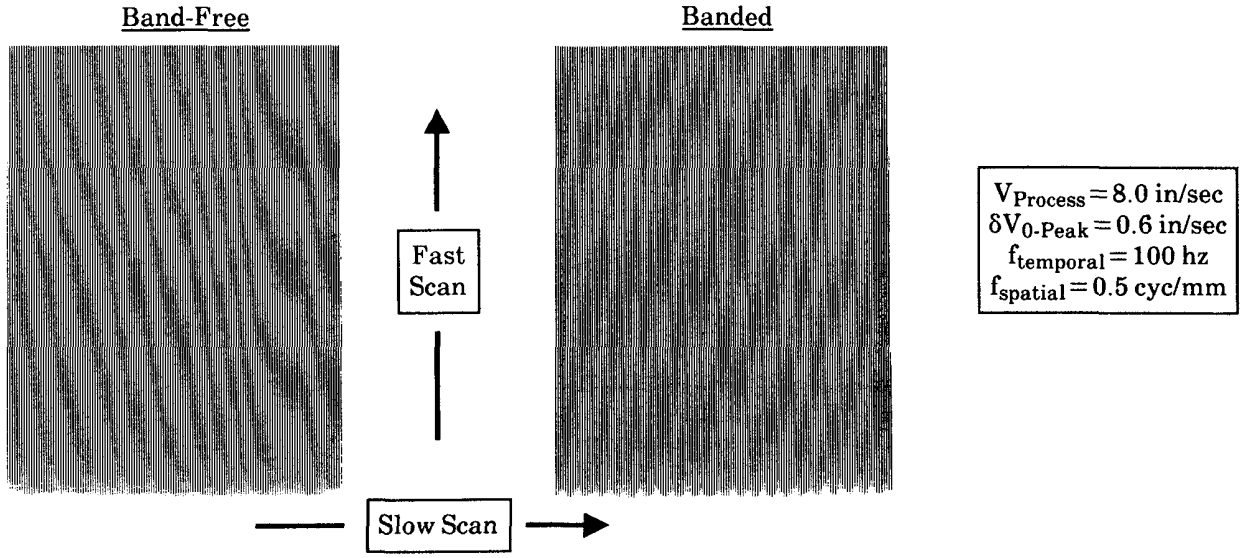

Figure 3. "Band-free" and banded prints of 1/150 inch wide vertical lines spaced 1/75 inches apart.

Opto-mechanical design curves are developed based on psychophysical experiments where a controlled amount of image motion is applied to halftone prints. The prints are judge by a panel of observers to determine whether or not banding is perceptible. Based on the results of these experiments, design curves of tolerable image motion can be plotted describing the "perceptibility threshold" in terms of velocity error vs. spatial frequency, $f_{spatial}$, as shown in Figure 4. Xerographic process parameters, line or halftone cell frequency, area coverage, and the psychophysics experimental technique will all effect the shape and amplitude of the perceptibility threshold. One common characteristic of most perceptibility threshold curves is that the minimum velocity error, δV_{min}, usually resides around a spatial frequency of 1.0 cycle/mm. This is attributed to human eye sensitivity maximizing at approximately the same spatial frequency.

The image science which studies banding is beyond the scope of this paper The mathematical treatment of this phenomena as well as the details of the psychophysical experiments used to formulate curves of tolerable image motion levels vs. frequency are discussed by Hamerly[1], Lama and Loce[2,3], and Costanza[4]. A failure criteria cited by Takiguchi, et.al.[5], which was adjusted for the specific xerographic process and process speed for this application, will be applied later in this paper to evaluate the design analysis performed on the ROS structure being analyzed.

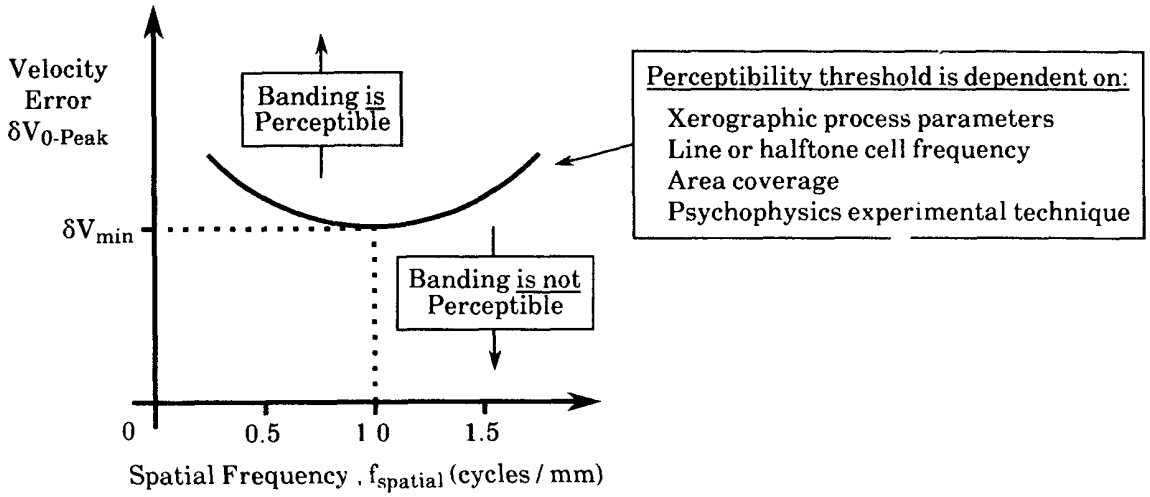

Figure 4 Typical print banding data showing the "perceptibility threshold".

5. ANALYSIS APPROACH

5.1 Structural dynamic fundamentals

Because a ROS experiences steady and intermittent structural excitations, it is necessary to evaluate the image motion response in both the frequency and time domain When the finite element model of the ROS is developed, the structural matrices will take the form of Equation 1, where [M], [B] and [K] represent the mass, damping and stiffness matrices, respectively, and $\{\ddot{x}\}$, $\{\dot{x}\}$, and $\{x\}$ represent acceleration, velocity and displacement vectors, respectively. The left hand side of the equation defines the structural properties while the right hand side of the equation defines the excitation properties imposed upon the structure. If the damping matrix and the right hand side of Equation 1 are equated to zero, the roots of the matrix equation, known as the "characteristic equation", can be found. These roots are known as the "eigenvalues" of the equation or the "natural frequencies "of the structure. The relative vector relationship between all displacement values in the equation at particular eigenvalues are known as the "eigenvectors" or the "modeshapes" of the structure

$$[M]\{\ddot{x}\} + [B]\{\dot{x}\} + [K]\{x\} = F \quad (1)$$

When the right hand side of the characteristic equation is equated to a frequency dependent forcing function as in Equation 2, a "frequency response" analysis is formulated. When the right hand side of the characteristic equation is equated to a time varying load as in Equation 3, a "transient response" analysis is formulated.

$$[M]\{\ddot{x}\} + [B]\{\dot{x}\} + [K]\{x\} = \{F\}\sin\omega t \quad (2)$$

$$[M]\{\ddot{x}\} + [B]\{\dot{x}\} + [K]\{x\} = \{F\}(t) \quad (3)$$

While the natural frequencies and modeshapes of a structure are essential dynamic properties, it is preferable to qualify the structural design by evaluation of image motion response and not the appearance of the relative modeshapes The recommended engineering procedure is to review the modeshape information of the response peak which exceeds a print quality failure threshold A design change based on good engineering judgment can be made to the finite element model. The response amplitudes can then be recalculated to verify the effectiveness of the design change.

The ideal time for an image motion response analysis to take place is in the early design stages of a laser printer. Since representative hardware is usually not available this early in product development, it is

difficult to know amplitudes and frequencies of steady structural loads, {F}sinωt, or the period and amplitude characteristics of intermittent transient loads, F(t). For similar machine architectures, accelerometer data has shown that the structural noise level present on machines in the vicinity of ROS mounting is usually less than 0.01 G's from 0 to 500 hertz as shown in Figure 5. As a conservative assumption for the frequency response analysis, a "white noise" spectrum of 0.01 G was applied across the entire frequency range and the resulting image motion response amplitude will be evaluated against banding thresholds

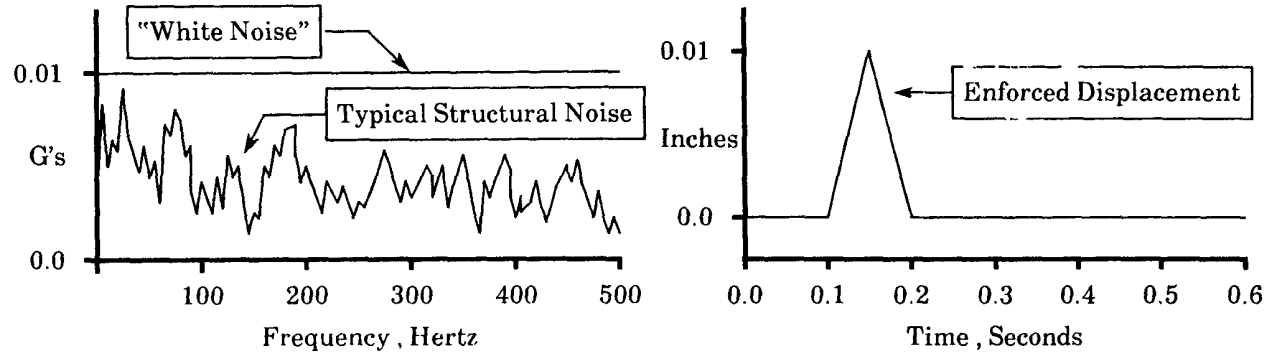

Figure 5 Frequency and time dependent loads applied to the analytical models.

To date less work has been done characterizing time dependent loads in laser printers. To demonstrate the transient analysis evaluation, an assumed 100 msec triangular enforced displacement with a peak amplitude of 0.01 inches was applied to the model. The enforced displacement, shown in Figure 5, is typical in shape to excitations of intermittent mechanical disturbances. When more is learned about the characteristics of time dependent loads the analysis can easily be updated.

5.2 Finite element model details

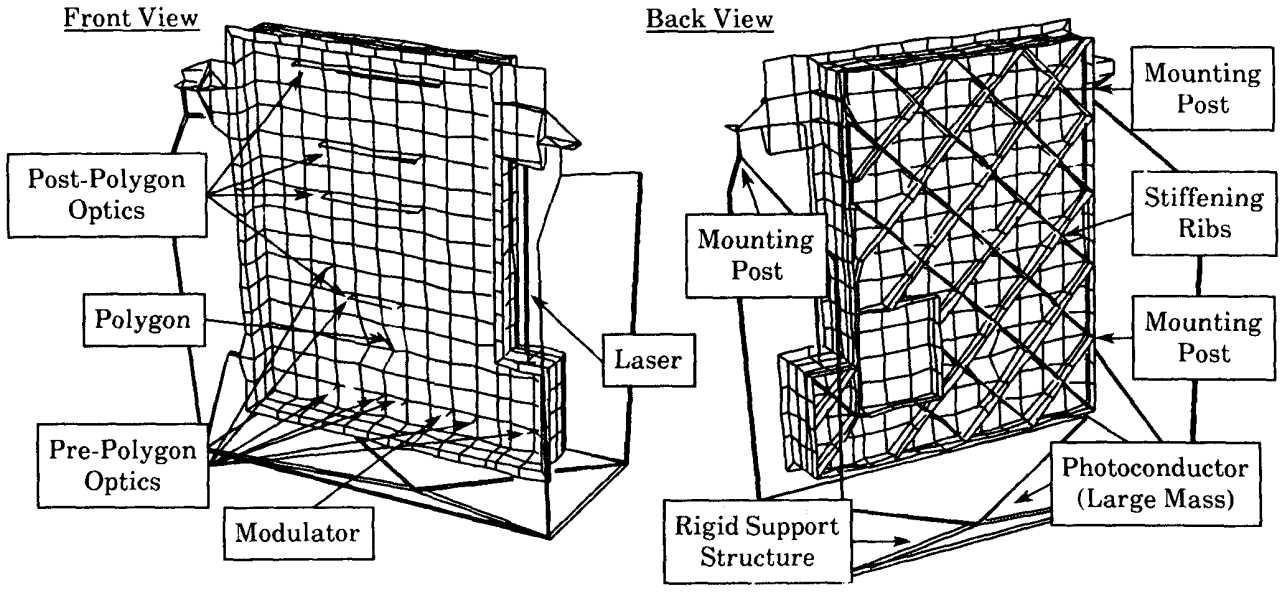

Figure 6 Finite element model of ROS showing the critical opto mechanical components.

The finite element model shown in Figure 6 was modeled using the PC pre-processor, FEMAP[6], analyzed using MSC/NASTRAN[7,8,9], and post-processed using MSC/GRASP[10]. The model consisted of 799 grid points, 704 quadrilateral and 34 triangular membrane-bending elements, 34 beam bending elements, and miscellaneous lumped mass and "rigid" elements which are internally formulated using constraint equations. The main body of the aluminum casting was modeled with the membrane-bending elements, and the mounting post was formulated with the beam elements. The pre- and post-polygon optics, polygon, modulator, laser and all optical standoffs were modeled with beam elements. The machine frame, which the ROS casting mounts to, and the photoconductor module were assumed rigid and modeled with rigid elements. A large mass was placed in the rigid structure so enforced motions representing structural excitations could be applied in the frequency and transient response analyses. From experience, the damping was assumed to be 5% of critical, and uniform over the entire structure and over the frequency ranges calculated.

The analysis was performed on a Vax 11/780 reconfigured by Intergraph, and took approximately 190 cpu minutes to complete a cold start of a normal modes run extracting the first 10 eigenvalues and eigenvectors Subsequent restarts of the modal solution for frequency and transient image motion response calculations usually ranged between 10 and 15 cpu minutes for 5 to 10 output quantities. The response calculations consisted of 600 frequency solutions at 0.5 hz. increments or 600 time solutions at 0.001 second increments, respectively.

5.3 Optical sensitivity coefficients

The sensitivity coefficients for individual optical component movement were developed at the center of the fast scan field using the ray trace computer program GENII-PC[11] The details of these calculations are beyond the scope of this paper In general, each optical component was perturbed in the 3 local translational and 3 local rotational directions, and the individual effects of these perturbations at the photoconductor surface were noted. The perturbations were in the order of 0 001 inch translation and 0.0001 radian rotation. This amount of perturbation is typical of structural response of laser printers and has subsequently been proven to reside in the linear range of the optical system The resulting normalized optical coefficients, A_1 through A_6, for each optical element are given in Table 1 for slow scan laser spot placement error.

Table 1. Normalized slow scan optical coefficients

Optical Element	A_1	A_2	A_3	A_4	A_5	A_6
Laser	0.0	0.0	-0.02	0.0	6.12	0.0
M_1	0.0	0.0	0.0	0.0	12 61	0.0
L_1	0.0	0.0	4.63	0 0	0 24	0.0
Modulator	0.0	0.0	0.0	0.0	1.24	0.0
L_2	0.0	0.0	-5.33	0.0	-0 04	0.0
L_3	0.0	0.0	0.0	0.0	-0.04	0.0
M_2	0.0	0 0	0.0	0.0	17.87	0.0
M_3	0.0	0.0	0.0	0.0	-7.47	0.0
L_4	0.0	0.0	-0.24	0.0	-0.07	0.0
Polygon	0.0	0.0	0.0	0.0	0.98	0.0
L_5	0.0	0.0	0.0	0.0	0.19	0.0
L_6	0.0	0.0	0.0	0 0	0.25	0.0
L_7	0.0	0.0	-1.505	0.0	0.53	0.0
M_4	0.08	0.0	3 505	0.0	40.09	0.0

The above coefficients were entered into the following image motion equation which was subsequently inserted into MSC/NASTRAN as a multi-point constraint equation referred to as an "MPC".

$$[A_1x+A_2y+A_3z+A_4\theta_x+A_5\theta_y+A_6\theta_z]_{Laser}+[A_1x+\ \ ..\ \ +A_6\theta_z]_{M_1}+$$
$$....+[A_1x+.....+A_6\theta_z]_{M_4}\ \ 1\ 0\ \delta_{Photoconductor}=IM_{Slow\ Scan} \qquad (4)$$

The output, $IM_{Slow\ Scan}$, is a measure of the resulting image motion The accuracy of Equation 4, within the finite element representation, was qualified by performing a static finite element solution. The ROS was

analytically displaced rigidly in space by known amounts, and the resulting spot motion was verified based on the input.

5.4 Finite element model validation

As with any finite element analysis, it is necessary to verify the validity of the model by empirical and/or other analytical means Experimental correlation of ±10.0% for finite element calculations is considered more than adequate for model validation The first empirical validation was a static bench test where the ROS was simply supported at the three (3) mounting locations on an optical bench using rigid standoffs. The polygon was locked at center scan and the output laser beam was imaged onto a silicon diode position sensor mounted at the image plane using another rigid standoff. A total static load of 10.0 lbs was incrementally applied at the free corner perpendicular to the plane of the casting (process direction), and slow scan spot motion and ROS mechanical deflection at the point of load application was recorded The empirical data was linear within the 10 lbs load range and is compared to the complementary analytical solution in Table 2.

Table 2. Comparison of analytical and empirical static results at 10 lbs load.

Location	NASTRAN	Bench Test	% Difference
Free Corner	0.0121 in	0.0119 in	-1.65
Position Sensor	0.0050 in	0.0046 in	-8.00

The ROS model was also validated with a modal test of an actual ROS casting. The ROS casting was suspended from "bungy cords" to simulate a free boundary condition. This was necessary in order to get noise free measurements so accurate modeshape data could be extracted. The results of this test for the first three (3) modes of vibration are given in Table 3 It must be pointed out that these frequencies are significantly higher then when the ROS is mounted in an actual machine structure. This is consistent with the fundamental behavior of beams and plates supported by kinematic mounts vs. free boundary conditions when comparing the first non-zero natural frequency

Table 3. Comparison of analytical and empirical natural frequency results.

Mode Number	NASTRAN	Modal Test	% Difference
f_1	169.1 hz	162 6 hz	3.84
f_2	372.4 hz	370.9 hz	-0.40
f_3	436.2 hz	416 8 hz	-4 45

The resulting modeshapes (not shown) also correlated very well It is reasonable to assume that the finite element model will be valid with any type of boundary conditions as long as frequency correlation has been demonstrated for the free boundary condition case.

6.RESULTS

Figure 7 shows the first 2 natural frequencies and modeshapes of the ROS. Judging these modeshapes, it appears that the mode at 43.2 hz would be more likely to cause banding problems than the mode at 79 4 hz since the motion of the ROS is predominantly in the process direction Review of the response data will qualify the previous speculation by showing which frequencies dominate the image motion response.

Reviewing the frequency response data in Figure 8 shows the 1st mode (43.2 hz.) is the dominant contributor to slow scan spot response based on a 0.01 G white noise excitation and could cause banding since the velocity value exceeds the perceptibility threshold. The modes at 74, 95, and 260 hz. show insignificant image motion response amplitudes when compared to the perceptibility threshold

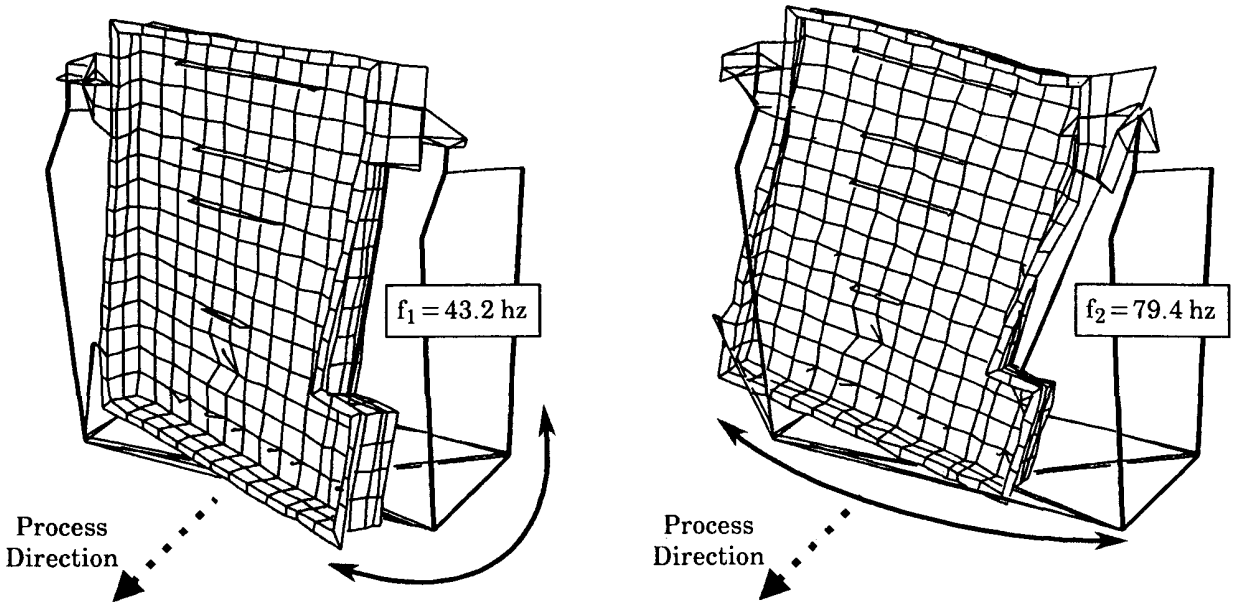

Figure 7 1st and 2nd structural modeshapes of the ROS casting

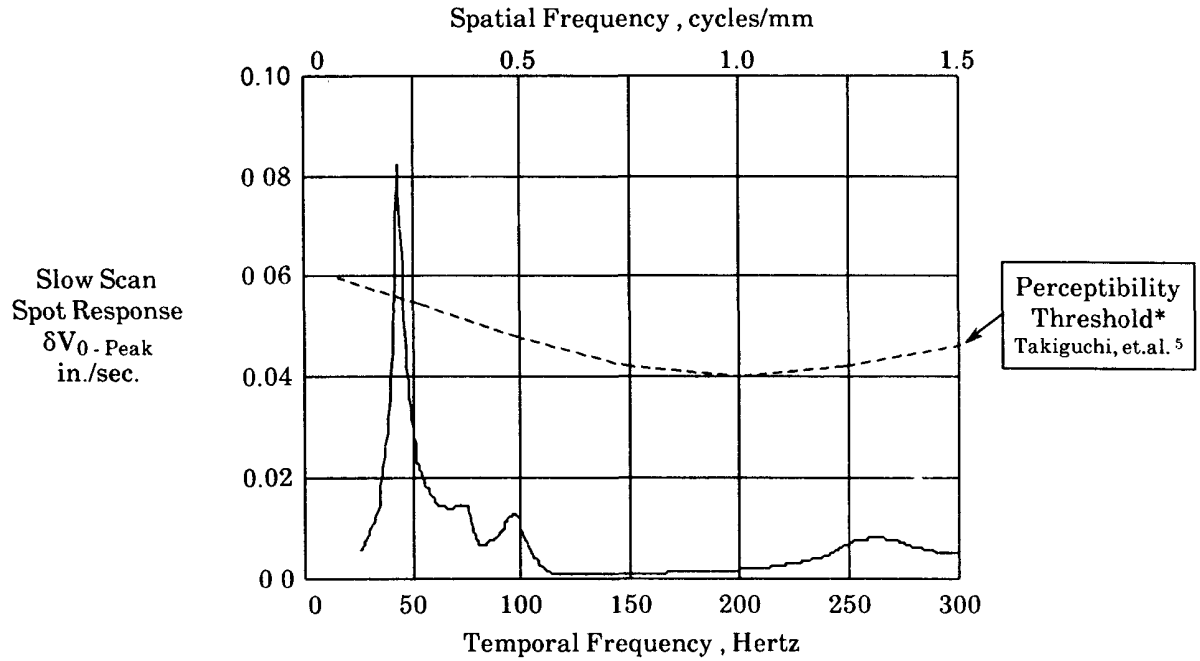

Figure 8. Spot response due to a 0.01g base excited white noise spectrum in the process direction.

* Perceptibility data was scaled to account for differences in xerographic processes.

Figure 9 shows transient image motion response in the slow scan direction. If the 0.01 inch enforced displacement is representative of a structural transient, the resulting response is dominated by the 43.2 hz. frequency. The perceptibility threshold data plotted in Figure 8 indicates that at 43 2 hz banding will become perceptible at 0.055 in./sec., 0-peak. This single frequency threshold is plotted in Figure 9 and the data indicates that about 10 peaks protrude outside of the perceptibility window. This means that 10 bands of varying darkness could occur in output prints.

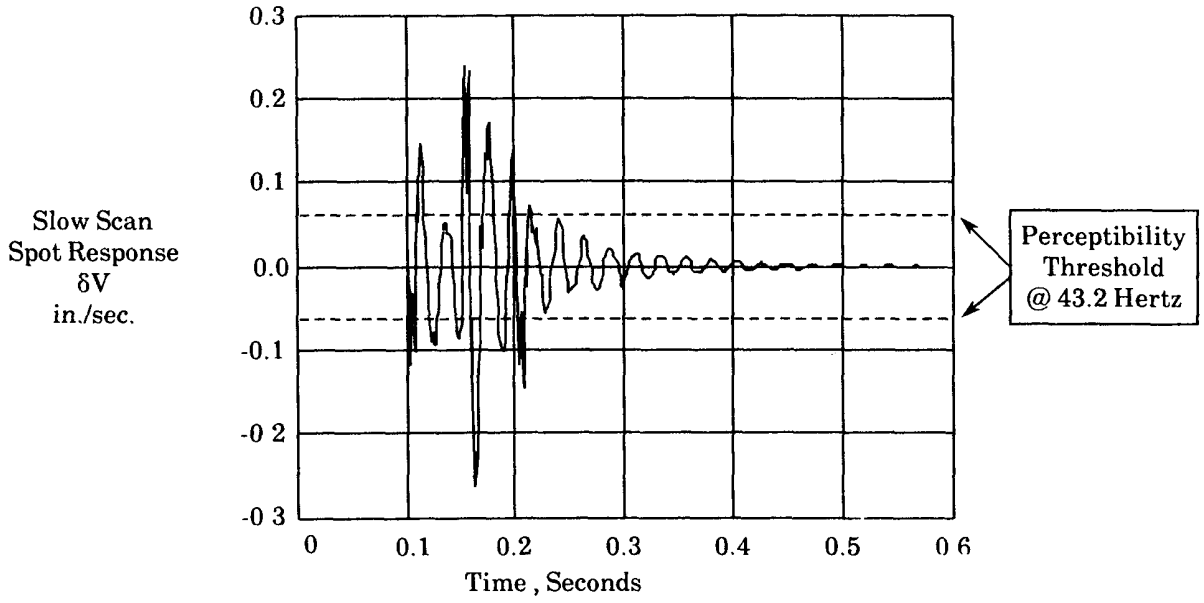

Figure 9. Spot response due to a triangular 0.01 inch - 100 msec enforced displacement in process direction

7. CONCLUSIONS AND RECOMMENDATIONS

A complete analysis method for the evaluation of structural image motion in laser printers has been developed and demonstrated Subsequent design modifications applied to the finite element model and followed up by additional image motion response calculations will eventually bring all response amplitudes below the perceptibility thresholds and qualify the design. While this technique has been demonstrated in the context of a design analysis tool, it could also be used later in laser printer program development if previously unpredicted image motion errors become perceptible or when design/cost optimization becomes an important engineering issue.

Future work in this area will include 1) the modeling of the machine frame, photoconductor module and all other major components which may effect image motion response, 2) benchmark measurement activity to better define steady and transient noise levels to be applied to the analytical model, and 3) optical coefficient development which would account for image motion response over the entire fast scan field

8. ACKNOWLEDGMENTS

The author would like to thank Mike Harrigan for coding and understanding the ROS optical formulation as well as his assistance in obtaining the optical sensitivity coefficients, and Jim Casella for performing the static and modal tests used for finite element model validation

9. REFERENCES

1) Hamerly, J.R., "Banding in the Printing of Digital Screens", Xerox internal report, 1984.

2) Lama, W. and Loce, R., "Effects of Vibration in Digital Printing Systems/Optical and Electrostatic Images", Xerox internal report, December 1985.

3) Loce, R., Lama, W. and Maltz, M., "Effects of Vibration in Digital Printers/Halftone Banding in Write White Xerographic Systems", Xerox internal report, December 1985.

4) Costanza, D., "Banding in Halftone Images, An Experimental Investigation", Xerox internal report, November 1988.

5) Takiguchi,T., et.al., "Effect of Photoreceptor Drum Rotational Speed Variation on Laser Beam Printer Halftone Reproduction", Presented at the SPSE Conference on Non-Impact Printing Technologies, San Fransisco, August, 1986.

6) "FEMAP User's Manual, Version 1.1", Enterprise Software Products, Inc , 1986

7) "MSC/NASTRAN User's Manual, Version 65", Vol.I and II, The MacNeal-Schwendler Corp , November 1985.

8) Joseph, J.A., "MSC/NASTRAN Application Manual, Vax Edition", Vol I and II, The MacNeal Schwendler Corp., November 1987.

9) Gockel, M.A ,editor, "MSC/NASTRAN, Handbook for Dynamic Analysis Version 63", The MacNeal-Schwendler Corp , June 1983

10) SanMarco, J.,"MSC/GRASP User's Manual, Version 3", The MacNeal-Schwendler Corp , November 1985.

11) "GENII-PC Reference Manual, Version 4 201", Genesee Computer Center, Inc., September 1986